Performance Evaluation of IEEE 802.11p Infrastructure-to-Vehicle Real-World Measurements with Receive Diversity

Georg Maier*, Alexander Paier† and Christoph F. Mecklenbräuker*
*Institute of Telecommunications, Vienna University of Technology, Vienna, Austria
†Kapsch TrafficCom AG, Vienna, Austria
Contact: gmaier@nt.tuwien.ac.at

***Abstract*—In this contribution, we present performance evaluation results for a multi-antenna receiver for Wireless Access in Vehicular Environments (WAVE) according to IEEE 802.11p. The analysis was performed by employing the Selection Combining (SC), the Equal Gain Combining (EGC) and the Maximum Ratio Combining (MRC) algorithms on recently carried out real-world measurement data. We show that a well-engineered diversity combining algorithm, applied to multi-antenna systems, significantly improves the reliability and robustness, even under poor receive conditions. The resulting performance enhancement compared to the single antenna regime in case of the frame success ratio (FSR) is increased up to 25 %. This is due to the fact that all available information from both antenna branches is utilized. Furthermore, we investigate the influence of different driving directions on the system performance.**

***Index Terms*—Vehicular communications, infrastructure-to-vehicle, IEEE 802.11p, receive diversity, measurements.**

I. Introduction

The growing number of traffic participants requires the use of intelligent transport systems (ITS). This important technology offers a wide range of novel services to increase the safety and traffic efficiency. Further, infotainment applications like real-time traffic information, in order to improve the traffic flow, are an important part for the integration of ITS into transport concepts. The exchange of information between the involved subscribers will be based on vehicle-to-infrastructure (V2I) and vehicle-to-vehicle (V2V) communication systems, summarized under the abbreviation vehicle-to-X (V2X). The vehicular communication radio environment is challenging due to the doubly-selective fading channel. Therefore much effort has to be invested in field-trials and/or simulations.

The appropriate standard for Wireless Access in Vehicular Environments (WAVE), namely IEEE 802.11p [1], mainly based on the Wireless Local Area Network (WLAN) IEEE 802.11a standard [2], and the approved amendment was published July 2010. The European Telecommunications Standards Institute (ETSI) developed a similar standard, called ITS-G5 [3]. Both technologies will work in the 5.9 GHz band, reserved for ITS.

Especially safety-related applications need a robust, low-latency and high-reliable data transmission between the involved nodes. On the other hand the complex roadway environment, the large number of moving vehicles and the randomly time-varying nature of the channel, poses a great challenge to V2X receivers. One way to improve the V2X communication is the use of multiple antennas at the receiver side. In this contribution we focus on the achievable improvement by the well-known receive diversity combining schemes in an infrastructure-to-vehicle scenario. The authors in [4] and [5] show, based on simulations, that multiple receive antennas significantly improve the performance in vehicular environments. The underlying data used for the evaluation in this paper are obtained from a vehicular measurement campaign within the national Austrian research project ROAD-SAFE [6]. A brief overview of the extensive measurement campaign and the utilized equipment with focus on the V2X MIMO testbed is given. The used hardware of the two-antenna testbed, called V2X MIMO testbed, consists of a digital signal processor (DSP) and a field programmable gate array (FPGA) combined with commercial off-the-shelf components. The software running on the V2X MIMO testbed and for the offline processing is implemented by our own. The presented results include the whole receiver process with receive diversity.

The remainder of the paper is organized as follows: the following section gives a brief overview of the IEEE 802.11p standard, the used measurement equipment, and the scenario used within the measurement campaign. Section III describes the receiver architecture and the used diversity schemes. The obtained results based on frame error ratio (FER), frame success ratio, and error distribution inside a frame are presented in Section IV. Finally, we draw conclusions in Section V.

II. System Description

In this section a short summary of the physical layer (PHY) and frame structure of the IEEE 802.11p standard is given. Furthermore, we present an overview of the main components of the measurement equipment, parameter settings, and also the environment.

A. System Architecture Overview

The IEEE 802.11p standard specifies a PHY based on orthogonal frequency-division multiplexing (OFDM) with 64

978-1-4577-1379-8/12/$26.00

subcarriers. Fifty-two subcarriers are used for actual transmission, where 48 subcarriers are suitable for carrying data. The remaining four pilot subcarriers are used to compensate the frequency and phase shifts. Four modulation schemes (BPSK, QPSK, 16-QAM, 64-QAM) and in addition three different coding rates of $1/2$, $2/3$, and $3/4$ are specified in the standard. With eight predefined combinations, a data rate range from 3 to 27 Mbit/s is reachable. The channel bandwidth of IEEE 802.11p is 10 MHz, which results in doubling all the OFDM timing parameters compared to the IEEE 802.11a standard. A summary of the most important system parameters is provided in Table I.

An IEEE 802.11p physical layer protocol data unit (PPDU) frame mainly consists of three different fields: PLCP (PHY convergence procedure) preamble, SIGNAL, and multiple data. The ten short training symbols, included in the first OFDM symbol of a frame, are used for automatic gain control (AGC) and coarse time and frequency synchronization. The short preamble is followed by two long symbols, in order to refine the frequency and time synchronization and further to obtain an initial estimate of the channel. The training structure is followed by the SIGNAL field and provides information about the used modulation scheme and coding rate for the data symbols and frame length, in order to set the correct decoding parameters. The SIGNAL field is encoded using BPSK with a coding rate of $1/2$. The first DATA symbol includes the 16 bit SERVICE field, whereas the first six bits are set to zero and used to synchronize the descrambler at the receiver.

TABLE I
IEEE 802.11p PHY PARAMETERS

Parameter	Value
Bandwidth	10 MHz
Subcarrier spacing	156.25 kHz
FFT size	64
Used, data, pilot subccariers	52, 48, 4
OFDM symbol duration	8 μs
Cyclic prefix duration	1.6 μs
Modualtion	BPSK, QPSK, 16-QAM, 64-QAM
Coding rate	$1/2, 2/3, 3/4$
Data rate	3, 4.5, 6, 9, 12, 18, 24, 27 Mbit/s

B. Measurement Campaign Overview

The used data in this paper was collected within the project ROADSAFE. In September 2011 a V2X measurement campaign on the highway A4 in the vicinity of Vienna, Austria, was carried out. This paper is focused on the evaluation of V2I measurements. The measurement location is located in the vicinity of the airport and an industrial area. This leads to an increased traffic, especially from big trucks. Also worth mentioning is a metallic curved-noise protection wall on one side of the highway. Three out of five roadside units (RSU) were located there. These facts imply a strong influence on the signal propagation. For the experiments five RSU provided by Kapsch TrafficCom (especially developed for outdoor usage) were installed on highway gantries. Two directional antennas were mounted on the top (approx. 7.1 m above the street) of each gantry, in order to cover all lanes in both directions.

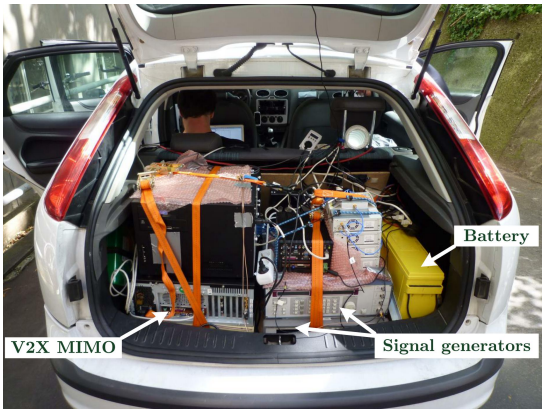

Fig. 1. Setup of the measurement equipment in the trunk of the test vehicle.

As onboard unit (OBU) the V2X MIMO testbed was used. The testbed and its additional equipment were installed in the trunk of a compact car (Ford Focus), see Fig. 1. The two surface mount antennas were placed on the outermost corners at the rear of the car roof.

The main components of the V2X MIMO testbed are a Digital Signal Processor (Texas Instruments TMS320C6416 DSP), a Field Programmable Gate Array (XILINX Virtex-5 XC5VSX50T FPGA) module from Sundance [7], and a mimoOn radio frequency (RF) frontend [8] placed in a standard personal computer. The RF frontend additionally needs two signal generators as clock source for the down conversion into the base band and for the analog-to-digital conversion of the received signal. On the FPGA the AGC, time and frequency synchronization with maximum ratio combining (MRC) are implemented. Further details about the implemented algorithms can be found in [9]. After the conversion from the analog base band into the digital domain the signal is down-sampled. The frequency compensated signal is stored in a First In - First Out (FIFO) memory on the FPGA and transferred into a 256 MByte SDRAM on the DSP module. If the memory is full or manually stopped by the user the recorded samples are saved on the hard disc drive. Due to the limited SDRAM size and the slow transfer rate between the single parts of the V2X MIMO testbed, a non-continuous data stream can be recorded for further offline processing.

A medium access control (MAC) service data unit (MSDU) packet length of 500 Byte was used. This corresponds with the used data rate of 6 Mbit/s (QPSK, coding rate $1/2$) to 555 Byte including all overhead, e.g. MAC Header and frame check sequence (FCS) field. The center frequency was set to 5900 MHz. During the whole measurement campaign the transmitter acts in the broadcast mode, i.e. no uplink signaling. All measurements were performed with an approximate

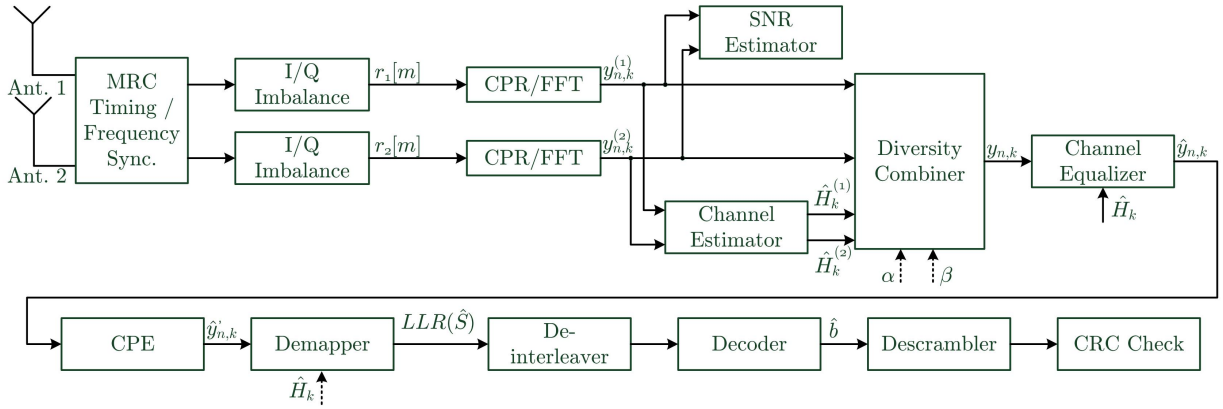

Fig. 2. IEEE 802.11p PHY dual antenna receiver block diagram

vehicle velocity of 80-100 km/h. The traffic conditions and environment during the measurement runs were documented by webcams, installed in the front and in the rear of the car. Further details of the entire measurement campaign are documented in [10].

III. Receiver Architecture

This section provides a detailed overview of the used receiver architecture and the applied diversity combining techniques. Figure 2 shows the block diagram of the two antenna system used for evaluating the measured data. As already mentioned in Section II-B the timing and frequency synchronization was performed online on the FPGA during the measurements with MRC and will not be discussed further.

A. System Architecture Overview

Due to the direct-conversion architecture and other non-ideal frontend components, an in- and quadrature phase (I/Q) imbalance estimation and compensation, according to [11], is introduced. Especially higher order modulation schemes are very sensitive to these kinds of non-idealities. After the cyclic prefix removal (CPR) the received time-domain signal is transformed back to the frequency-domain using a 64-point fast Fourier transformation (FFT). The Signal-to-Noise Ratio (SNR) estimation is performed by using the algorithm presented in [12]. The SNR is an imported parameter for several diversity combining schemes, i.e. selection combining (SC) and maximum ratio combining (MRC).

The averaged least squares algorithm

$$\hat{H}^{(i)}_k = \frac{1}{2}\left(\frac{y^{(i)}_{LP1,k}}{x_{LP,k}} + \frac{y^{(i)}_{LP2,k}}{x_{LP,k}}\right), \tag{1}$$

is used for the initial channel estimation and is calculated for each antenna branch separately, except for SC. Where $y^{(i)}_{n,k}$ is the received data at antenna (i) at time instance n and subcarrier index k. Whereas the local stored long preamble (LP) is denoted by $x_{LP,k}$. This algorithm uses the fact that the long preamble consists of two identical parts, in order to increase the reliability of the channel estimate. The diversity combiner and channel equalizer are discussed in the next subsection. Due to non-perfect synchronization, a common phase error (CPE) can still remain. An estimate for the n-th symbol is given by

$$\hat{\phi}_n = \arg\left(\sum_{k\in\wp} \hat{y}_{n,k} p^*_{n,k}\right), \tag{2}$$

where $\wp$ denotes the set of pilot subcarriers and $p^*_{n,k}$ the complex conjugate of the transmitted pilots. The estimated rotation is corrected by multiplying all subcarriers with $\exp(-\jmath\hat{\phi}_n)$.

The demapper calculates log-likelihood ratios (LLRs) for each coded bit, according to [13], and after deinterleaving the data is decoded with the soft-input VITERBI [14] algorithm. The descrambled data is used to calculate the FCS, a 32-bit CRC (cyclic redundancy check) number, corresponding to IEEE 802.11p. This recalculated FCS is compared with the received CRC, in order to determine a valid or erroneous frame.

B. Diversity Combining Techniques

The principal of receive diversity is to combine multiple versions of the transmitted signal into an improved single signal. Assuming the same information reaches the receiver on statistically independent channels, it is possible to reduce the influence of time- and/or frequency selective channels on the transmitted signal. There exist several methods that can be used to combat fading, e.g. spatial, temporal, or frequency diversity. In our case, a so called single-input multiple-output (SIMO) system is used to achieve spatial diversity. In the receiver, a linear diversity combiner is implemented that is defined by

$$y_{n,k} = \alpha y^{(1)}_{n,k} + \beta y^{(2)}_{n,k}, \tag{3}$$

where α and β are the weighting factors according to one of the following combining scheme. There are basically two ways for combining signals from multiple diversity branches, namely selection and combining diversity.

1) Antenna Selection or Selection Combinig (SC): As the name already indicates, only one signal branch is further processed. The decision, which antenna stream is used, is based, in our case, on the amplifier gain set by the AGC. If the same gain is set for both antennas, the SNR estimate is used to make a decision which frame is further processed. After selection, zero forcing (ZF) equalization is done on the selected antenna channel response.

2) Equal Gain Combining (EGC): There are in principal two ways to perform EGC. In the first case both branches are added without phase compensation, the so-called incoherent EGC (iEGC), according to

$$y_{n,k} = y_{n,k}^{(1)} + y_{n,k}^{(2)}\,, \tag{4}$$

or in the second case coherently EGC (cEGC)

$$\begin{aligned} y_{n,k} = {} & y_{n,k}^{(1)} \exp\left(-\jmath \arg \hat{H}_k^{(1)}\right) \\ & + y_{n,k}^{(2)} \exp\left(-\jmath \arg \hat{H}_k^{(2)}\right)\,, \end{aligned} \tag{5}$$

with phase compensation. The channel compensation value used by the ZF equalizer for iEGC is given by

$$\hat{H}_k = \hat{H}_k^{(1)} + \hat{H}_k^{(2)} \tag{6}$$

and if cEGC is applied by

$$\hat{H}_k = |\hat{H}_k^{(1)}| + |\hat{H}_k^{(2)}|\,. \tag{7}$$

3) Maximum Ratio Combining (MRC): In the case of MRC the signals from both antenna branches are phase and amplitude aligned corresponding to

$$y_{n,k} = \alpha y_{n,k}^{(1)} \left(\hat{H}_k^{(1)}\right)^* + \beta y_{n,k}^{(2)} \left(\hat{H}_k^{(2)}\right)^*\,. \tag{8}$$

The two weighting factors α and β depend on the used amplifier gain and the estimated SNR value of each antenna stream. The resulting combined channel state information

$$\hat{H}_k = \alpha|\hat{H}_k^{(1)}|^2 + \beta|\hat{H}_k^{(2)}|^2 \tag{9}$$

is not only used by the ZF equalizer but also by the demapper.

IV. Results

In this section we present the obtained results after the evaluation process. As mentioned in Section II-B, we selected a data rate of 6 Mbit/s, that corresponds to QPSK modulation and a coding rate of $1/2$. The PSDU length was set to 555 Byte which corresponds to a frame duration of 784 μs, including preambles and signal field. Figure 3 shows the results for the infrastructure-to-vehicle scenario with different receive diversity techniques applied to the recorded signals. The fact that the plotted E_B/N_0 values are only in the range of 8-18 dB is that outside this range, too few frames were received, in order to allow a fair comparison. The blue line with circles and the green line with squares represent the results for antenna $\mathrm{A}^{(1)}$ and $\mathrm{A}^{(2)}$ without combining. SC results are plotted in red with diamonds. The two EGC techniques iEGC and cEGC use upward-pointing triangles and downward-pointing triangles as markers, whereas the MRC result is presented by a black solid line with a star. The two dashed black lines are explained below.

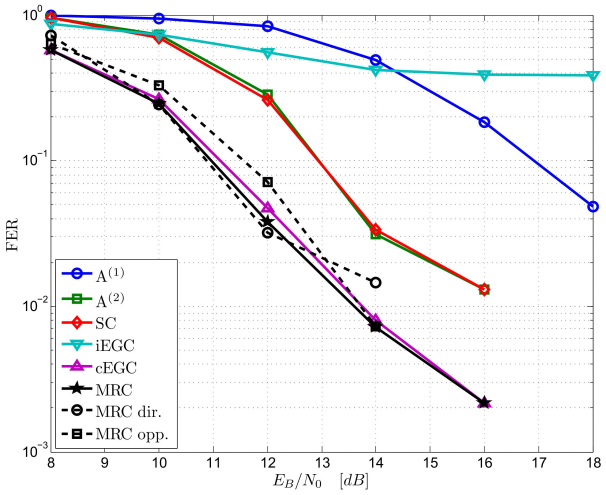

Fig. 3. FER results with different combinig schemes for the infrastructure-to-vehicle scenario.

One of the first eye-catching results is the quite high performance difference for single antenna evaluation. This was somehow expected, since we have observed this behavior during the evaluation in case of synchronization and packet detection of the ROADSAFE 2010 measurement campaign data in [9]. A reason for this might be different antenna radiation pattern due to the mounting and/or more likely due to impairments or non-idealities in the two-antennas RF frontend chains.

Now, we have a closer look on the results if one of the combining schemes, described in Section III-B, is applied. The expectation in case of SC is a slightly performance improvement compared to a SIMO configuration. In our case the result shows that SC has a similar behavior as the $\mathrm{A}^{(2)}$ case. On one hand this is due the fact that SC discards copies of the received signal and on the other hand the performance of $\mathrm{A}^{(1)}$ is much worse compared to $\mathrm{A}^{(2)}$.

The next step in adding complexity, in order to improve the performance, is EGC. By adding the two branches without any further processing we observe an improvement in the lower E_B/N_0 regime compared to $\mathrm{A}^{(1)}$ but not $\mathrm{A}^{(2)}$. For E_B/N_0 values of approximately 14 dB it looks like that iEGC reaches an error floor. A potential reason for this behavior is the imperfect frequency and time synchronization and destructive interference in the combining process. This is mitigated by considering a phase alignment into the combining process, in order to get a constructive addition. This is reached by using cEGC that results in a much better performance. A similar behavior is achieved by applying MRC, which was not expected. On the one hand at higher E_B/N_0 values, where we expect a better performance of MRC, fewer frames were recorded and almost all of them are decodable. On the other hand, comparing Eq. (5) and Eq. (8), we note that MRC uses only the additional amplitude information. Moreover,

the advantage of using the whole available information is degraded by imperfection, e.g. incorrect carrier frequency offset estimation, in the receiving process.

As a first outcome, we preliminarily conclude. The achievable diversity gain at a FER of 10 % is in the range of 2 dB if MRC or cEGC is used compared to $A^{(2)}$ or SC and 5.8 dB in contrast to $A^{(1)}$.

Another viewpoint is to have a look at the frame success ratio (FSR). An overview is shown in Table II, where two different definitions are listed. The overall FSR (oFSR) is calculated by the number of successfully decoded frames divided by the entire received frames. Whereas the decodable FSR (dFSR) uses, as the name suggests, only the successfully decodable frames within this evaluation setting. This implies that e.g. MRC is not able to successfully decode 3 % of the frames that are decodable with one of the other schemes. With a first glance look we see that the conclusions drawn based on the FER are confirmed. While in the case of SC a small improvement of 2 % is observed. Nevertheless, a performance improvement by up to 25 % is achievable with the use of an appropriate diversity combining scheme compared to a single-input single-output (SISO) system.

TABLE II
OVERALL AND DECODEABLE FSR WITH AND WITHOUT ANTENNA DIVERSITY.

	$A^{(1)}$	$A^{(2)}$	SC	iEGC	cEGC	MRC
oFSR	28 %	63 %	65 %	42 %	87 %	88 %
dFSR	30 %	69 %	71 %	46 %	96 %	97 %

Now, we want to utilize the knowledge about the transmitted data and parse the received data according to possible byte errors. The outcome is plotted in Fig. 4 for antenna $A^{(2)}$ and MRC. Where the x-axis represents the byte location inside the frame (MSDU + MAC header length) and the E_B/N_0 values assigned to the y-axis. The intensity color shows the probability that at a certain E_B/N_0 value, an error at a dedicated location inside the frame occurs. The two white bars at the beginning correspond to two counter values, i.e. 12-bit sequence control field and a 4 Byte user implemented one. These are different for each frame and therefore not really provable to be correct. This is also true for FCS at the end of each frame and thus it is also not included. It should further be noted that especially at higher E_B/N_0 values also errors occur but in lower scale and as a result of the color code they are not visible. It is observed that starting at a length of approximately 350 Byte the possibility of an error highly increases. A possible explanation for this is that the channel state information is only estimated once at the beginning of a frame and therefore is outdated at the end. The same behavior, but of course in a weaker form, is observed in the case of MRC. The scaling factor is reduced by a factor of six, in order to highlight this behavior. These two plots also show the potential of using more than one antenna and an appropriate combining scheme. Figure 4 also highlights the use of more sophisticated receiver algorithms, especially for the channel estimation and equalization, due to the time-invariant channel.

As already mentioned in Section II-B the RSU antennas were mounted to cover all lanes in both directions and therefore a similar performance, regardless of the driving direction, was expected. Finally, we discuss whether the driving direction influences the FSR. In Table III the FSR for four different evaluation settings are presented. Beside the MRC also both single antenna cases, $A^{(1)}$ and $A^{(2)}$, are listed. The abbreviations dir. and opp. stands for driving in the direction below the gantry or on the opposite driving lanes. As mentioned earlier in this section in Fig. 3 two black dashed curves are plotted also with this labeling. It has to be noted that this result represents the data obtained when using RSU 4 only. The objective of using only a single RSU is that there are three measurement repetitions in each direction available, in order to ensure a fair comparison between the two driving directions. In Table III we show the overall FSR for the whole available measurement data separated by the driving direction, labeled with All RSUs, and for three individual RSUs. RSU 1 and RSU 2 were chosen because of at least two repetitions in each direction and to ensure that the overall result is not depending on a single RSU. For almost all analyzed data the oFSR is higher when passing directly below the gantry except for RSU 2 $A^{(2)}$ and RSU 1 $A^{(1)}$. With the help of the video documentation we identified that in at least one measurement run a big metal truck was driving in front which influences the result.

TABLE III
FSR FOR DIFFERENT DRIVING DIRECTIONS AND RSUS

	All			RSU 4		
	$A^{(1)}$	$A^{(2)}$	MRC	$A^{(1)}$	$A^{(2)}$	MRC
oFSR	28 %	63 %	88 %	26 %	56 %	85 %
oFSR dir.	35 %	68 %	91 %	36 %	70 %	91 %
oFSR opp.	23 %	60 %	86 %	15 %	41 %	78 %

	RSU 2			RSU 1		
	$A^{(1)}$	$A^{(2)}$	MRC	$A^{(1)}$	$A^{(2)}$	MRC
oFSR	32 %	70 %	90 %	41 %	79 %	95 %
oFSR dir.	40 %	69 %	92 %	31 %	87 %	97 %
oFSR opp.	21 %	72 %	88 %	48 %	75 %	93 %

V. CONCLUSION

This contribution provides an overview of different receive diversity techniques in an infrastructure-to-vehicle scenario based on real-world measurements. The presented results show that the performance is improved if an appropriate combining scheme, e.g. maximum ratio combining, is applied to a single-input multiple-output vehicular communication system. We also showed that with the use of coherent equal gain combining or maximum ratio combining the frame success ratio is increased by 25 % or a diversity gain of 2 dB is obtained at

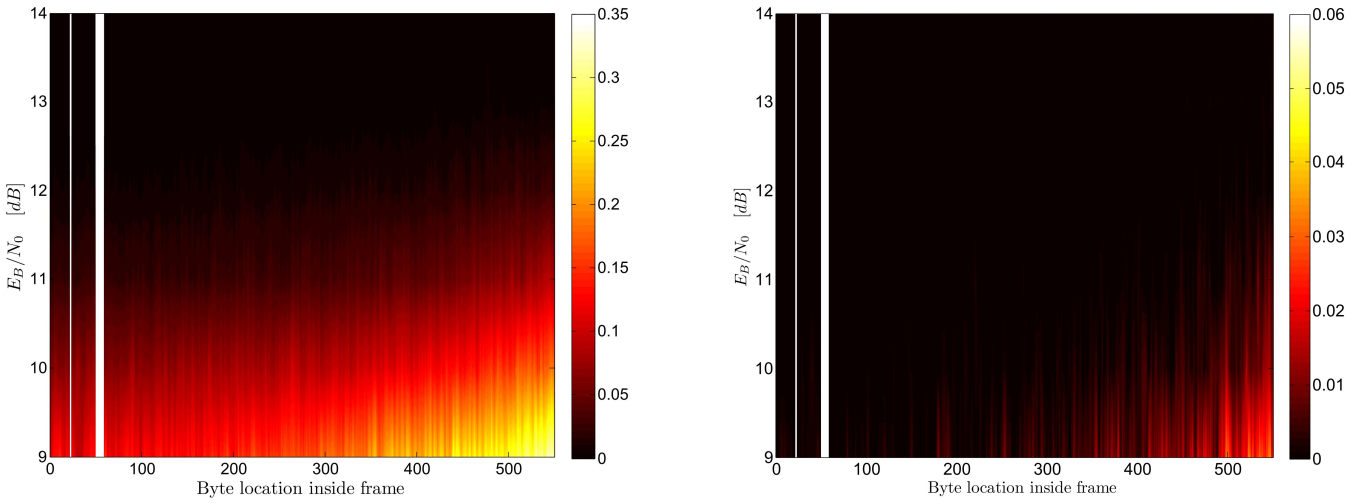

(a) Result for $A^{(2)}$

(b) Result with MRC

Fig. 4. Byte error occurrence (color coded) as a function of position inside the frame and E_B/N_0 with and without diversity.

a frame error ratio of 10 %, compared to the single antenna case. Since all available information is exploited, combining diversity, i.e. coherent equal gain combining and maximum ratio combining, leads to an improved performance. This improvement comes with a higher implementation complexity compared to selection diversity or using only a single antenna.

Furthermore, we analyzed and discussed the byte error distribution within the received frames. The obtained results indicate that larger frames lead to significantly increased error probabilities. This argument also holds for maximum ratio combining but of course in weaker form. We stress that the message length shall be chosen with care for avoiding retransmissions when the channel estimator is based only on the preamble. This is even more necessary for safety related messages requiring dependable connectivity.

We also showed that the driving direction (lane below the roadside unit or lane next to the roadside unit in opposite direction) has an influence on the performance in an infrastructure-to-vehicle scenario. This is denoted by an 5 % lower frame success ratio when driving in opposite direction.

ACKNOWLEDGMENT

This work has been funded by the Christian Doppler Laboratory for Wireless Technologies for Sustainable Mobility The financial support by the Federal Ministry of Economy, Family and Youth and the National Foundation for Research, Technology and Development is gratefully acknowledged. We acknowledge Kapsch TrafficCom AG for supplying the RSUs and the Federal Ministry for Transport, Innovation, and Technology of Austria (BMVIT) for granting a test license in the 5.9 GHz band.

REFERENCES

[1] *IEEE Standard for information technology-Telecommunications and information exchange between systems-Local and metropolitan area networks-Specific requirements Part 11: Wireless LAN Medium Access Control (MAC) and Physical Layer (PHY) Specifications - Amendment 6: Wireless Access in Vehicular Environments*, IEEE Standard 802.11p-2010, Jul. 2010.

[2] *IEEE 802.11a, Part 11: Wireless LAN Medium Access Control MAC and Physical Layer PHY Specifications High-speed Physical Layer in the 5 GHz Band*, IEEE Std. 802.11a-1999(R2003), Jun. 2003.

[3] *Intelligent Transport Systems (ITS); European profile standard for the physical and medium access control layer of Intelligent Transport Systems operating in the 5 GHz frequency band*, ETSI Standard ETSI ES 202 663, Rev. V1.1.0, Jan. 2010.

[4] J. Nuckelt, H. Hoffmann, M. Schack, and T. Kürner, "Linear diversity combining techniques employed in Car-to-X communication systems," in *Proc. 73rd IEEE Vehicular Technology Conference, (VTC2011-Spring)*, Budapest, Hungary, May 2011, pp. 1–5.

[5] A. Bourdoux, H. Cappelle, and A. Dejonghe, "Channel tracking for fast time-varying channels in IEEE802.11p systems," in *Proc. IEEE Global Telecommunications Conference, (GLOBECOM 2011)*, Houston, Texas, USA, Dec. 2011, p. 6.

[6] ROADSAFE. [Online]. Available: http://www.ftw.at/projects/roadsafe

[7] Sundance Multiprocessor Technology. [Online]. Available: http://www.sundance.com/

[8] mimoOn. [Online]. Available: http://www.mimoon.de/

[9] G. Maier, A. Paier, and C. F. Mecklenbräuker, "Packet detection and frequency synchronization with antenna diversity for IEEE 802.11p based on real-world measurements," in *Proc. International ITG Workshop on Smart Antennas, WSA 2011*, Aachen, Germany, Feb. 2011, pp. 1–7.

[10] V. Shivaldova, A. Paier, T. Paulin, G. Maier, P. Fuxjäger, A. Alonso, D. Smely, B. Rainer, and C. F. Mecklenbräuker, "Overview of an IEEE 802.11p PHY performance measurement campaign 2011," in *2nd Management Committee Meeting of COST IC1004*, no. IC1004 TD(11) 02056, Lisbon, Portugal, Oct. 2011, p. 6.

[11] I. Held, O. Klein, A. Chen, and V. Ma, "Low complexity digital IQ imbalance correction in OFDM WLAN receivers," in *Proc. IEEE 59th Vehicular Technology Conference, VTC 2004-Spring*, vol. 2, Milan, Italy, May 2004, pp. 1172–1176.

[12] G. Ren, H. Zhang, and Y. Chang, "SNR estimation algorithm based on the preamble for OFDM systems in frequency selective channels," *IEEE Transactions on Communications*, vol. 57, no. 8, pp. 2230–2234, Aug. 2009.

[13] F. Tosato and P. Bisaglia, "Simplified soft-output demapper for binary interleaved COFDM with application to HIPERLAN/2," in *Proc. IEEE International Conference on Communications, ICC 2002*, vol. 2, New York, NY, USA, Apr./May 2002, pp. 664–668.

[14] A. J. Viterbi, "Error bounds for convolutional codes and a asymptotically optimum decoding algorithm," *IEEE Transactions on Information Theory*, vol. IT-13, no. 2, pp. 260–269, Apr. 1967.